Journal of New Materials for Electrochemical Systems 17, 235-242 (2014)

Effect of Rare Earth Elements on the Structure and Electrochemical Properties of $La_{0.63}R_{0.2}Mg_{0.17}Ni_{3.1}Co_{0.3}Al_{0.1}$ Alloy Electrodes

Zhijie Gao[1,†], Xiaodong Zheng[1], Ping Du[1] and Yongchun Luo[2,*]

[1]Department of Chemical Engineering, Binzhou University, Binzhou, 256600, P R China
[2]Department of Materials Science and Engineer, Lanzhou University of Technology, Lanzhou, 730050, P R China

Received: April 24, 2014, Accepted: May 05, 2014, Available online: November 25, 2014

Abstract: *Hydrogen storage alloys $La_{0.63}R_{0.2}Mg_{0.17}Ni_{3.1}Co_{0.3}Al_{0.1}$ (R = La, Ce, Pr, Nd, Y, Sm, Gd) based on A_2B_7 type were prepared by induction melting method. The alloys were annealed at 1173K during a week in a sealed stainless steel tube. The structure and the electrochemical properties of the annealed alloys have been studied systematically by XRD, EPMA and electrochemical studies. The alloys structure consists mainly of Ce_2Ni_7-type (SG: $P6_3/mmc$) La_2Ni_7 phase as well as minor Gd_2Co_7-type (SG: R-3m) phase, $LaNi_5$ ($CaCu_5$-type, SG:P6/mmm) phase. It is resulted that $La_{0.65}Y_{0.2}Mg_{0.15}Ni_{3.1}Co_{0.3}Al_{0.1}$ alloy exhibited the maximum electrochemical discharge capacity of 381.2 mAh·g^{-1}. The best cycling stability was obtained with the $La_{0.65}Gd_{0.2}Mg_{0.15}Ni_{3.1}Co_{0.3}Al_{0.1}$ based alloy. This stability measured as the capacity retention rate at the 100th cycle (S_{100}) was the highest for this sample (92.7%). The variation of the high rate discharge ability with the alloy composition. Its displayed a wave-like change. Firstly it increased from 24.5% (R = La) to 78.4% (R = Ce), then decreased to 14.4 % (R = Sm), and increased again to 63.8% with R = Gd.*

Keywords: Rare earth elements; Alloy structure; Unit cell volume; Equilibrium pressure; Electrochemical properties

1. INTRODUCTION

Nowadays more interesting has been attracted on the application of hydrogen storage alloys for the "Hydrogen Energy economy" [1]. Rare-earth-based AB_5-type alloy and Zr-based Laves phase alloy have been commercialized successfully as Ni/MH secondary cell negative materials [2,3]. However, the extensive applications are also limited by low capacity of AB_5-type and difficult activation of Laves phase alloy materials [4,5]. Many electrode with powerful and reversible electrochemical redox reactions are regarded as promising energy storage materials [6].

Since the use of $LaMg_2Ni_9$, La_2MgNi_9 and $La_5Mg_2Ni_{23}$ compounds were reported as hydrogen storage materials [7-9], ternary R-Mg-Ni (R = rare earth metals) compounds have been studied for their superior hydrogen storage properties corresponding binary AB_n (n = 2-5) compounds [10-23]. On the one hand, the compounds have the remarkable advantages of high hydrogen capacity, moderate hydrogen equilibrium pressure as well as low contents of expensive elements; On the other hand, unknown structural properties raise the need for basic, crystallographic research. Recently, details about the structures of $Ce_2Ni_7H_{4/4.7}$ [24,25], $Ce_2MgCo_9H_{12}$ [26], $La_2Ni_7H_{6.5}$ [27], $La_2Ni_7H_x$ (x = 6.4, 10.8) [11], $La_{1.5}Mg_{0.5}Ni_7H_{9.3}$ [28], $La_{1.66}Mg_{0.34}Ni_7D_{8.8}$ [29] and $La_4MgNi_{19}H(D)_x$ [14, 16, 17, 19] have been published, but little is known about the $(R, Mg)_2Ni_7$-H system. Moreover, this data left open questions concerning about the influence of the R substitution on the structural and electrochemical characteristics of such compounds. Furthermore, previous research revealed that the crystal structure of a binary R_2Ni_7 compound is size dependent; viz., the Ce_2Ni_7-type structure is stable for larger R-atomic radii, the Gd_2Co_7-type structure is preferred for smaller M-atomic radii, and both structures coexist in the case of medium-sized R-atomic radii [30]. This phenomenon also raises the questiones as to whether the crystal structure of multicomponent $(R, Mg)_2Ni_7$ compounds is also similar to binary R_2Ni_7 compounds on size dependent. To clarify these two questions, the structure stabilities of Ce_2Ni_7- or Gd_2Co_7-type were studied by comparing their relative amounts in the $(La_{1.66}Mg_{0.34})Ni_7$-based compounds after partial substitution by different elements. On the basis of the $(La_{1.66}Mg_{0.34})Ni_7$ compound, Ce, Pr, Nd, Y, Sm and Gd are used as smaller substitutes

To whom correspondence should be addressed:
Email: *luoyc@lut.cn, †gaozhijie1983@126.com
Phone: +86-931-297-4813; Fax: +86-931-280-6962

for La, respectively, to change the average A-atomic radius. Similarly, Ni is partially replaced by Co and Al to increase the average B-atomic radius because Ni has the smallest atomic radius among transition metals.

From a hydrogen storage point of view, absorb and desorb hydrogen reaction under moderate conditions was also happened on $La_{1.66}Mg_{0.34}Ni_7$ with a Ce_2Ni_7-type structure,which is regarded as a representative reaction of $(R, Mg)_2Ni_7$ compounds [29]. Its hydride formation enthalpy is about −31.4 kJ/mol H_2, which is close to −30 kJ/mol H_2 for the $LaNi_5$−H_2 system [31]. However, electrochemical properties of $(La_{1.66}Mg_{0.34})Ni_7$-based compounds have not been reported to date. Moreover, the effects of partial substitution for La in the $(La_{1.66}Mg_{0.34})(Ni,Co,Al)_7$ compound on the electrochemical hydrogen absorption and desorption also interest us because alloying is an effective method to improve hydrogen storage properties. Hence, the electrochemical properties of $La_{0.63}R_{0.2}Mg_{0.17}Ni_{3.1}Co_{0.3}Al_{0.1}$ (R=La, Ce, Pr, Nd, Y, Sm, Gd) compounds were finally investigated.

2. EXPERIMENT

Hydrogen storage alloys with various formulations ($La_{0.63}R_{0.2}Mg_{0.17}Ni_{3.1}Co_{0.3}Al_{0.1}$ R=La, Ce, Pr, Nd, Y, Sm, Gd) were prepared by induction melting approach at 0.4 MPa of Ar. atmosphere. The ingots were wrapped in a thallium (Ta) foil, sealed in stainless steel tubes under Ar pressure (0.1 MPa) and annealed for a week at 1173K. Due to the high vapor pressure of Mg element, 10 wt.% excess of Mg element was necessary during melting. The purity of all elements was above 99 wt.%.

The annealed alloys were crushed mechanically into powder (<38μm) for x-ray diffraction (XRD) measurements and powder from 54μm to 61μm for electrode test. XRD measurements were performed on a Rigaku D/max-2400 diffractometer with Cu radiation and a power of 40kV×150mA. The patterns were recorded over the range from 15° to 90° in 2θ by step of 0.02°. Then the collected data were analyzed by the Rietveld method [32] using Fullprof 2K software [33] to get the lattice parameters and phase abundance.

The microscopic structure and the composition for annealed alloys were examined by Electron probe microanalyzer (EPMA-1600).

Alloy electrodes were prepared by cold pressing the mixture of alloy power and carbonyl nickel power at the weight ratio of 1:3 under 20MPa pressure to form a pellet of 10mm in diameter. Electrochemical measurements were performed at 293K in a standard open tri-electrode electrolysis cell consisting of alloy electrode, a sintered $Ni(OH)_2$/NiOOH anode and a Hg/HgO reference electrode immersed in 6M KOH electrolyte. Each electrode was discharged to cut-off potential –0.6V Vs. Hg/HgO reference electrode. Electrodes were charged/discharged at 60mAg^{-1} when activated; Electrodes were charged/discharged at 300mAg^{-1} when examined for cyclic stability. Because of low hydrogen absorption/desorption plateau for La-Mg-Ni alloy system [10], a self-discharge problem can be ignored if the time for testing of electrodes is not very long [21]. Therefore, P-C isotherms could be determined by electrochemical method according to the Nernst equation [22]:

$$E\text{eq(Vs. Hg/HgO)}=-0.9305-0.02955\text{Log}(P_{eq}) \text{ at } 293\text{K} \quad (1)$$

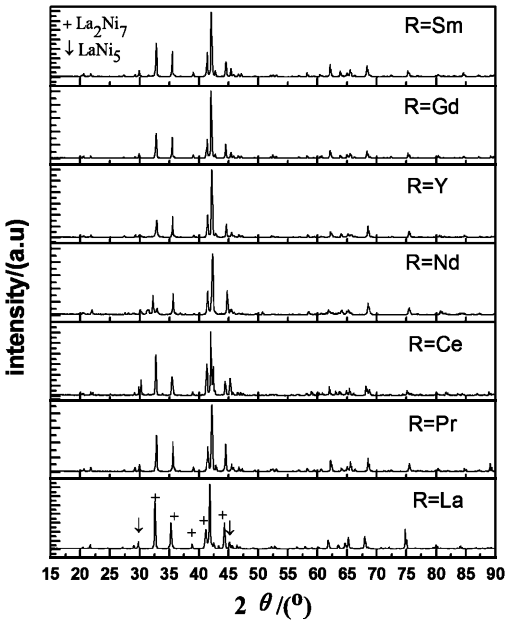

Figure 1. XRD patterns for $La_{0.63}R_{0.2}Mg_{0.17}Ni_{3.1}Co_{0.3}Al_{0.1}$ alloys.

Where the equilibrium potential (Eeq) was determined by alternately performing the following operation: (a) a pulse discharge of 10$mAhg^{-1}$ with 50mAg^{-1} current density. (b) a rest period (about 20 minutes) for the potential to become constant. The high rate dischargeablity (HRD) was determined by examining the discharge capacity at various discharge current density and defined as the following equation:

$$HRD = \frac{C_d}{C_{60}} \times 100\% \quad (2)$$

Where C_d is the discharge capacity at I_d current density, C_{60} is the discharge capacity at I_{60} current density.

To investigate the electrocatalytic activity and kinetics character of alloy electrodes, linear polarization, anodic polarization and hydrogen diffusion in alloy bulk were performed on CHI660A electrochemical work station after alloy electrodes were activated. The linear polarization, anodic polarization, and Tafel polarization curves were measured by scanning the electrode potential at a rate of 0.1mVs^{-1} from –5 to 5mV (Vs. open circuit potential), 5mVs^{-1} from open circuit potential to –0.45V (Vs. Hg/HgO reference electrode) and 1mVs^{-1} from -1.1 to -0.3V at 50% depth of discharge (DOD), respectively.

3. RESULT AND DISCUSSION

3.1. Alloy structure

Fig.1 shows the XRD patterns for $La_{0.63}R_{0.2}Mg_{0.17}Ni_{3.1}Co_{0.3}Al_{0.1}$ (R=La, Ce, Pr, Nd, Y, Sm, Gd) alloys. The alloys consist mainly of La_2Ni_7 (Ce_2Ni_7-type, SG: $P6_3/mmc$) phase and minor $LaNi_5$ ($CaCu_5$-type, SG:P6/mmm) phase from Jade 5.0 analysis. Fig.2 shows the Rietveld refinement patterns of $La_{0.63}R_{0.2}Mg_{0.17}Ni_{3.1}Co_{0.3}Al_{0.1}$ (R = La, Gd) alloy. Structure charac-

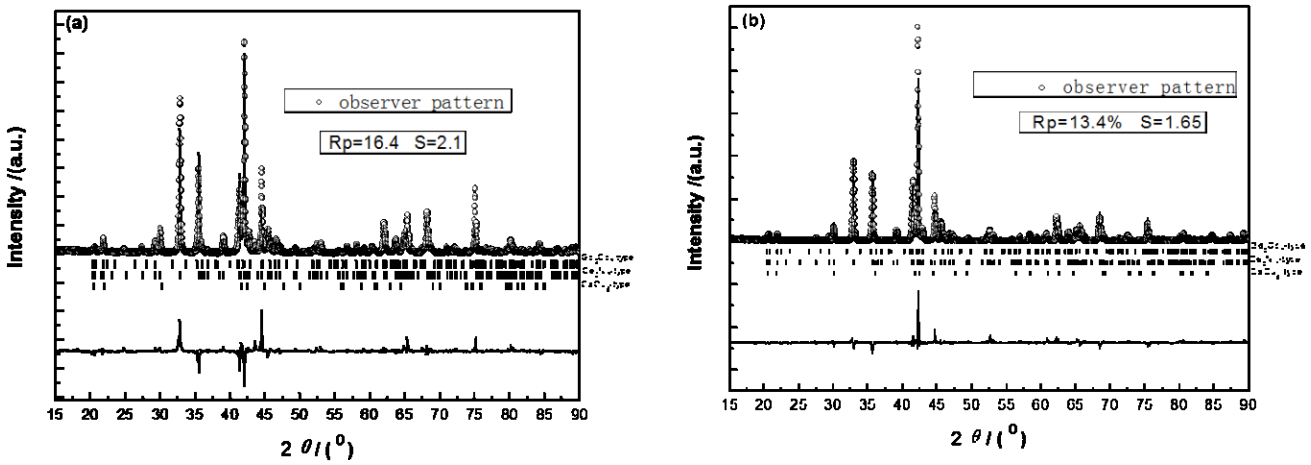

Figure 2. Rietveld refinement patterns for $La_{0.63}R_{0.2}Mg_{0.17}Ni_{3.1}Co_{0.3}Al_{0.1}$ alloy: (a) R = La, (b) R = Gd.

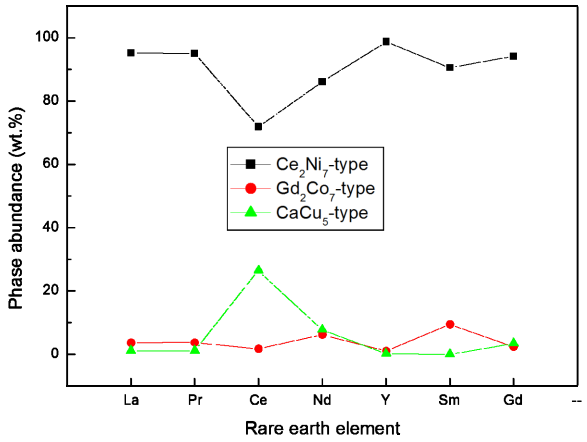

Figure 3. Phase abundance variation curves for $La_{0.63}R_{0.2}Mg_{0.17}Ni_{3.1}Co_{0.3}Al_{0.1}$ alloys.

teristics of different R-substituted alloys are tabulated in Table 1 and the evolution of phase abundance vs. rare earth atoms' radii are pictured in Fig.3. Based on the above data, the crystal structure of $La_{0.63}R_{0.2}Mg_{0.17}Ni_{3.1}Co_{0.3}Al_{0.1}$ seems to retain the hexagonal Ce_2Ni_7-structure type, which is different from the crystal structure of a binary R_2Ni_7 compound [30]. This may be ascribed to the content of rare earth. For $La_{0.63}R_{0.2}Mg_{0.17}Ni_{3.1}Co_{0.3}Al_{0.1}$ alloys, although Ce, Pr, Nd, Y, Sm and Gd are used as smaller substitutes for La, respectively, to change the average A-atomic radius, Ce_2Ni_7-type structure almost don't change.

The back scattered electron (BSE) image of $La_{0.63}R_{0.2}Mg_{0.17}Ni_{3.1}Co_{0.3}Al_{0.1}$ (R=La, Pr, Y, Gd) and are shown in Fig 4. A light grey area (α) and black area (β) can be seen in Fig 4 ((a) - (d)). The WDS analyses in Fig 4 show that the light grey (α) and black area (β) correspond to A_2B_7- and AB_5-type phase, respectively. The results are consistent with those obtained from XRD.

Table 1. Characteristics of phases for $La_{0.63}R_{0.2}Mg_{0.17}Ni_{3.1}Co_{0.3}Al_{0.1}$ annealed alloys.

Sample	Phase	Space Group	Lattice constants (Å)				Phase abundance (wt.%)
			a	c	V	c/a	
	$(La,Mg)_2(Ni,Co)_7$	R-3m	5.098	36.662	825.227	7.191	3.61
R = La	$(La,Mg)_2(Ni,Co)_7$	$P6_3/mmc$	5.061	24.438	542.148	4.829	95.23
	$La(Ni,Co)_5$	P6/mmm	5.018	4.034	87.964	0.804	1.16
	$(La,Mg)_2(Ni,Co)_7$	R-3m	4.949	36.470	773.608	7.369	3.74
R = Pr	$(La,Mg)_2(Ni,Co)_7$	$P6_3/mmc$	5.032	24.399	535.040	4.849	95.11
	$La(Ni,Co)_5$	P6/mmm	5.056	4.063	89.954	0.804	1.16
	$(La,Mg)_2(Ni,Co)_7$	R-3m	5.338	37.945	936.514	7.108	1.73
R = Ce	$(La,Mg)_2(Ni,Co)_7$	$P6_3/mmc$	5.049	24.401	538.616	4.833	71.84
	$La(Ni,Co)_5$	P6/mmm	5.019	3.996	87.163	0.796	26.43
	$(La,Mg)_2(Ni,Co)_7$	R-3m	5.037	35.689	784.152	7.085	6.21
R = Nd	$(La,Mg)_2(Ni,Co)_7$	$P6_3/mmc$	5.048	24.392	538.268	4.832	86.10
	$La(Ni,Co)_5$	P6/mmm	5.019	3.998	87.195	0.797	7.69
	$(La,Mg)_2(Ni,Co)_7$	R-3m	5.031	36.469	799.431	7.249	1.08
R = Y	$(La,Mg)_2(Ni,Co)_7$	$P6_3/mmc$	5.029	24.302	532.299	4.832	98.7
	$La(Ni,Co)_5$	P6/mmm	5.016	4.013	87.444	0.800	0.22
	$(La,Mg)_2(Ni,Co)_7$	R-3m	4.784	36.336	720.141	7.595	9.45
R = Sm	$(La,Mg)_2(Ni,Co)_7$	$P6_3/mmc$	5.043	24.361	536.434	4.831	90.54
	$La(Ni,Co)_5$	P6/mmm	5.035	4.030	88.486	0.800	0.00
	$(La,Mg)_2(Ni,Co)_7$	R-3m	5.079	36.541	816.295	7.195	2.40
R = Gd	$(La,Mg)_2(Ni,Co)_7$	$P6_3/mmc$	5.039	24.351	535.507	4.833	94.16
	$La(Ni,Co)_5$	P6/mmm	4.995	4.089	88.359	0.819	3.44

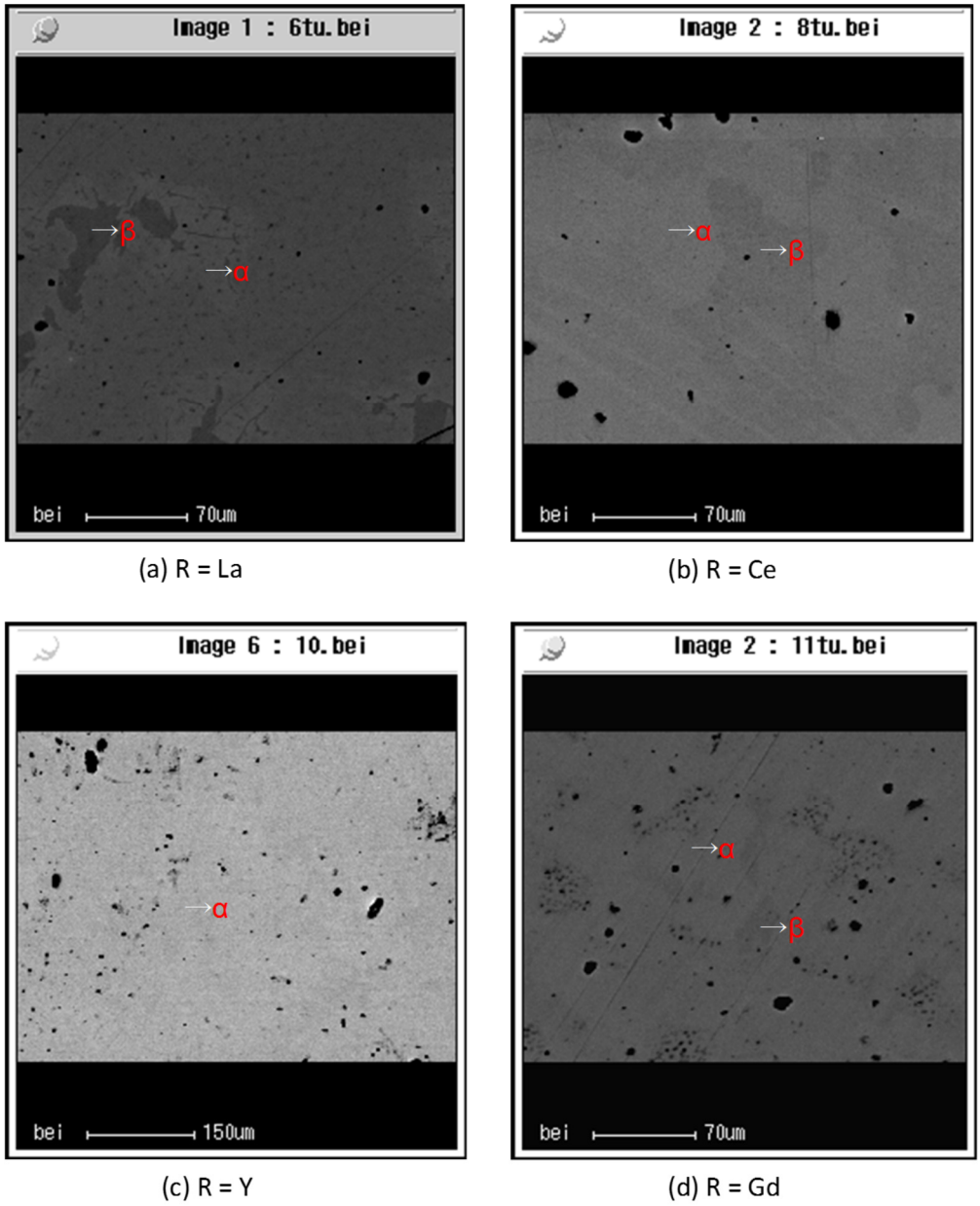

Figure 4. Back scattered electron images for $La_{0.63}R_{0.2}Mg_{0.17}Ni_{3.1}Co_{0.3}Al_{0.1}$ alloys (a) R = La (b) R = Ce (c) R = Y (d) R = Gd.

3.2. Thermodynamic characteristics

Fig.5 shows the electrochemical desorption P-C isotherm for different R-substituted alloys, and Table 2 summarizes the desorption characteristics of different alloys. The plateaus of the hydrogen desorption isotherms increase by substituting Ce~Gd at La sites. It can be seen that the desorption plateau became flatter and wider little by little with Pr~Gd substituted, which could be related with unit cell volume of alloys. From Table 2, it is obvious that the plateau slope firstly decrease from 1.694 (R = La) to 1.226 with Y substituted, and then increase to 1.752 (R = Pr), then decrease to 1.226 by substituting Y at La sites, finally increase from 1.575 (R = Sm) and 1.534 (R = Gd). In addition, the hydrogen content (H/M) also increased with Pr~Gd substituted and reached maximum (1.02H/M) at R=Pr, Y. Among the seven alloys, none-substituted alloy has the lowest hydrogen storage capacity.

The equilibrium hydrogen pressure is believed to correlate to the Ce_2Ni_7-structure and the unit cell volume of alloys; the tendency is the increase of the equilibrium pressure with the decreased unit cell volum. When the unit cell volume is in the range of 532-539 $Å^3$, the equilibrium pressure ranges from 0.045 to 0.01 atm (Fig. 5). The hydrogen-storage alloys that are used as the negative electrode materials must have a proper equilibrium pressure range in their gaseous PCT curves. If their hydrogen-desorption pressure plateau does not be in this range, the potential reversible electrochemical capacity must be smaller.

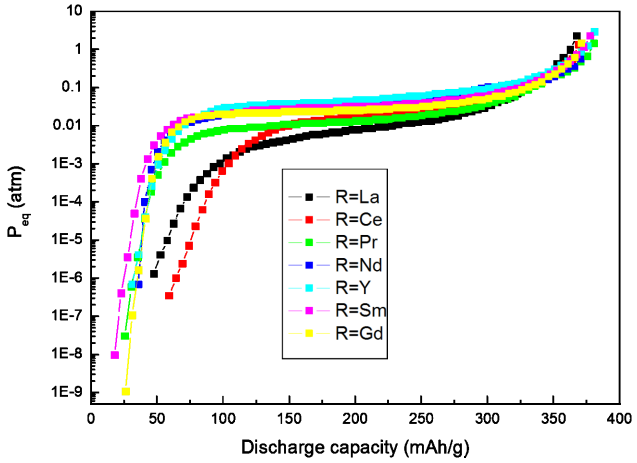

Figure 5. Electrochemical desorption P-C isotherms of $La_{0.63}R_{0.2}Mg_{0.17}Ni_{3.1}Co_{0.3}Al_{0.1}$ alloys at 293K.

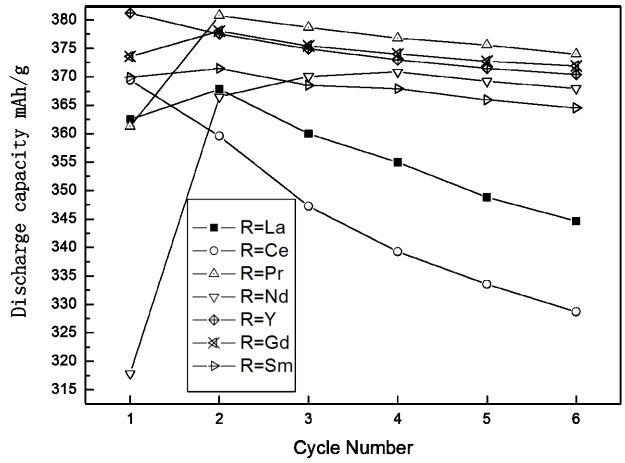

Figure 6. Activation curves of $La_{0.63}R_{0.2}Mg_{0.17}Ni_{3.1}Co_{0.3}Al_{0.1}$ annealed alloy electrodes with 60mAg^{-1} charge-discharge current density at 293K.

3.3. Charge/discharge characteristics

Fig.6 shows the activation curves of different alloy electrodes, and Table 3 summarizes electrochemical performance of different alloy electrodes. It can be found that all of alloy electrodes exhibited good activation properties; four charge/discharge cycles were

Table 2. Hydrogen desorption characteristics for $La_{0.63}R_{0.2}Mg_{0.17}Ni_{3.1}Co_{0.3}Al_{0.1}$ annealed alloys.

Alloy	H/M	Pd (atm)	Plateau slope*
R=La	0.98	0.007	1.694
R=Ce	0.98	0.014	1.508
R=Pr	1.02	0.012	1.252
R=Nd	0.99	0.037	1.255
R=Y	1.02	0.043	1.226
R=Sm	1.00	0.029	1.575
R=Gd	1.00	0.025	1.534

Pd is the pressure at midpoint of desorption hydrogen process.
Plateau slope* =Log(p|x(H)/x(M)=0.75/P|x(H)/x(M)=0.25)

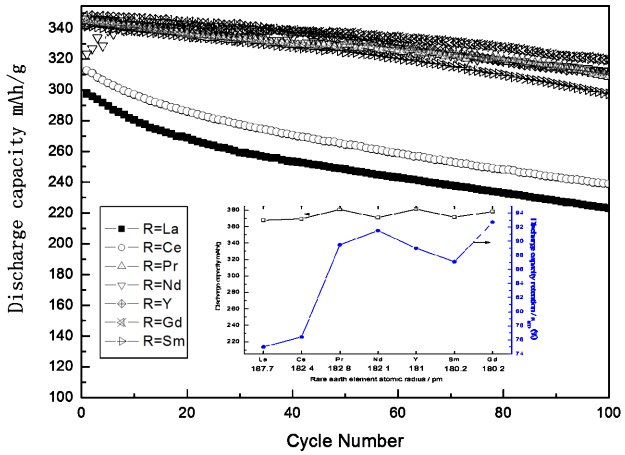

Figure 7. Cyclic stability curves of $La_{0.63}R_{0.2}Mg_{0.17}Ni_{3.1}Co_{0.3}Al_{0.1}$ annealed alloy electrodes with 300mAg^{-1} charge-discharge current density at 293K.

enough to activate electrodes. The capacity increases after La is substituted by Ce ~ Gd, The maximal discharge capacity of Y-substituted alloy increases to 381.2mAhg^{-1}, increasing by 3.6% compared with the $La_{0.83}Mg_{0.17}Ni_{3.1}Co_{0.3}Al_{0.1}$ alloy.

Cycling stability of metal hydride electrode is an important factor to cycle life of Ni/MH batteries. It can be seen from Fig. 7 that slope of cycle life profiles becomes smaller with Pr ~ Gd substitution for La, indicating that the cycle life is improved. In order to illustrate cycling stability, capacity retention rate at the 100th cycle (S_{100}) is calculated as the ratio of C_{100}/C_{max}, and is listed in Table 3. Table 3 shows that Pr- ~ Gd-substitution causes an increase in S_{100}. Gd substitution improves cycle life significantly with S_{100} increasing from 75 to 92.7%.

The following reasons are responsible for substituting La with R enhancing the cycle stability of the alloy. Firstly, the positive impact of R substitution on the cycle stability of the alloy is primarily ascribed to the refinement of the grains caused by such substitution. It has come to light that the fundamental reasons for the capacity decay of the electrode alloy are the pulverization and oxidation of the alloy during charging-discharging cycle. The lattice stress and the expansion of the cell volume, which are inevitable when hydrogen atoms enter into the interstitial sites of the lattice, are the real driving force that leads to the pulverization of the alloy. The anti-pulverization capability of the alloy basically depends on its grain size [34]. Therefore, it is understandable that the cycle stability of

Table 3. Summary of electrochemical performance for $La_{0.63}R_{0.2}Mg_{0.17}Ni_{3.1}Co_{0.3}Al_{0.1}$ annealed alloy electrodes at 293K

Sample	N	C_{max}(mAhg^{-1})	HRD_{900}(%)	S_{100}(%)	I_0(mAg^{-1})	I_L(mAg^{-1})
R=La	2	367.85	24.5	75	179.18	1100
R=Ce	1	369.417	78.4	76.4	354.31	3190
R=Pr	2	380.784	58.5	89.5	230.04	1860
R=Nd	4	370.867	21.8	91.5	133.29	1270
R=Y	1	381.2	16.7	89	91.14	740
R=Sm	2	378.029	14.4	87.1	102.7	620
R=Gd	2	371.47	63.8	92.7	141.21	1130

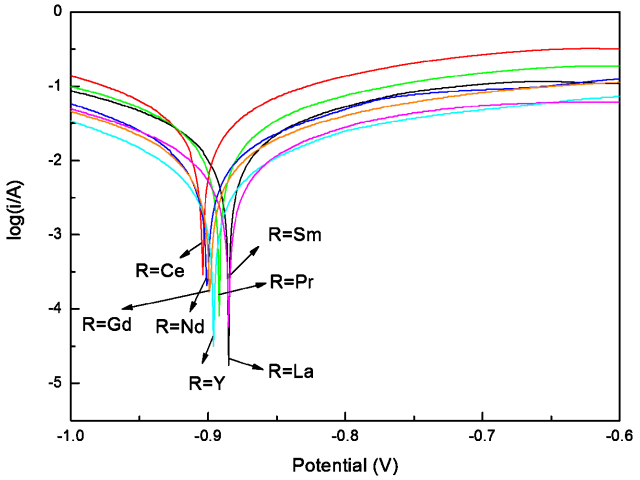

Figure 8. Tafel polarization curves of $La_{0.63}R_{0.2}Mg_{0.17}Ni_{3.1}Co_{0.3}Al_{0.1}$ alloy electrodes at 293K.

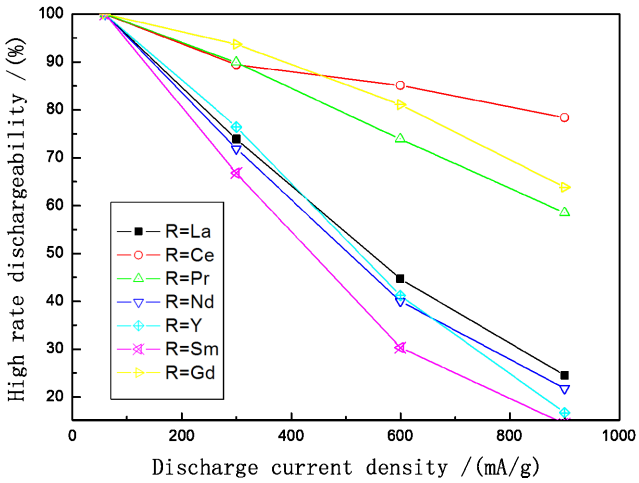

Figure 9. High rate dischargeability (HRD) curves of $La_{0.63}R_{0.2}Mg_{0.17}Ni_{3.1}Co_{0.3}Al_{0.1}$ alloy electrodes at 293K.

the alloy increases with R substitution. Secondly, it should be noticed that the main phase of the different alloys was Ce_2Ni_7-type phase. At the same time, the phase aboundance of $LaNi_5$ phase originated from substituting La with R is beneficial for improving cycle stability of the alloy due to an undoubted that $LaNi_5$ phase possesses much higher electrochemical cycle stability than $(La, Mg)_2(Ni,Co)_7$ phase. Thirdly, during charge/discharge process, rare earth elements tend to diffuse towards alloy surface, and the disproportion is determined by atom concentration and cell volume. The unit cell volume should be in the range of 532-539 $Å^3$ for electrochemical application. On the other hand, the different corrosion rates of different rare earth element may become an important factor to the cyclic stability of alloy electrode. Fig.8 shows the Tafel polarization curves of different alloy electrodes at 293K. The corrosion rates (v) can be attained according to the following equation [35]:

$$v = (3.6\times10^{7})i_{corr}w/(nF) \quad (3)$$

Where v and i_{corr} are proportional. So according to the corrosion current can be judged. Value of i_{corr} and E_{corr} is also listed in Table 4, it can be seen that the corrosion rates and corrosion potential of these alloys are in order: Ce > La > Sm > Pr > Y > Nd > Gd, respectively. It can be concluded that the alloy for R = Gd have a property of corrosion resisting, which is consistent with that of the cyclic stability basically. That is Nd and Gd substitution can suppress oxidation of the alloy elements and help to keep original structure of the alloys. As a result, the Nd- and Gd-substituted alloy have better cycling stability.

Table 4. Tafel fitting date of the $La_{0.63}R_{0.2}Mg_{0.17}Ni_{3.1}Co_{0.3}Al_{0.1}$ alloys at 293K

Sample	i_{corr} / (mA · cm^{-2})	E_{corr} / V
R=La	3.333	-0.8847
R=Ce	9.569	-0.9038
R=Pr	2.243	-0.8922
R=Nd	2.055	-0.9008
R=Y	2.242	-0.8957
R=Sm	2.333	-0.8847
R=Gd	1.573	-0.8990

Calculated based on Tafel equation, i_{corr} is the corrosion current density, E_{corr} the corrosion potential

3.4. Electrochemical kinetic characteristics

Fig.9 shows the high rate dischargeability (HRD) curves of different alloy electrodes. It can be found that Ce, Pr and Gd substitutions for La are beneficial to HRD of the alloys. High rate dischargeability at discharge current density of 900mAg^{-1} (HRD_{900}) is listed in Table 3. Ce substitution brings prominent improvement in HRD, and HRD_{900} of Ce-substituted alloy reaches 78.4%, which is 220% higher than that of the original alloy (24.5%).

It is known that HRD characteristic stands for overall kinetic properties, HRD can be influenced mainly by charge-transfer on surface of alloy electrodes and hydrogen diffusion in alloy bulk. The linear polarization and anodic polarization curves of $La_{0.63}R_{0.2}Mg_{0.17}Ni_{3.1}Co_{0.3}Al_{0.1}$ (R=La, Ce, Pr, Nd, Y, Sm, Gd) alloy electrodes are plotted in Fig. 10 and 11, respectively. Table 3 summarized the kinetic characteristics of alloy electrodes. Exchange current density (I_0) can be calculated according to the following equation [36]:

$$I_0 = \frac{RTI_d}{F\eta} \quad (4)$$

Where R is the gas constant, T is absolute temperature, I_d is the applied current density, F is the Faraday constant and η is the total overpotential. It is known that exchange current density (I_0) and limiting current density (I_L) are the other parameters to describe the kinetic characteristic of alloy electrodes. I_0 can be used to judge the speed of charge transfer on surface of alloy electrodes. I_L can be influenced by charge transfer, hydrogen diffusion and passivation of active composition. As shown in Table 3, The Ce- and Pr-substituted alloys have much larger exchange current density I_0, indicating their higher charge transfer rate at electrode surface.

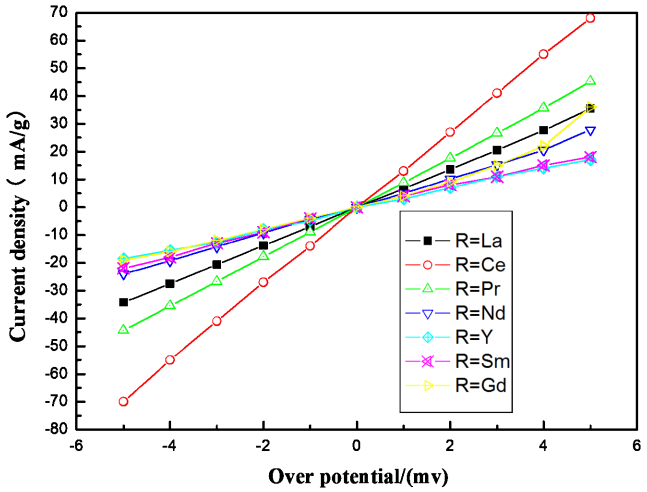

Figure 10. The Linear polarization curves of $La_{0.63}R_{0.2}Mg_{0.17}Ni_{3.1}Co_{0.3}Al_{0.1}$ alloy electrodes at 50% DOD and 293K.

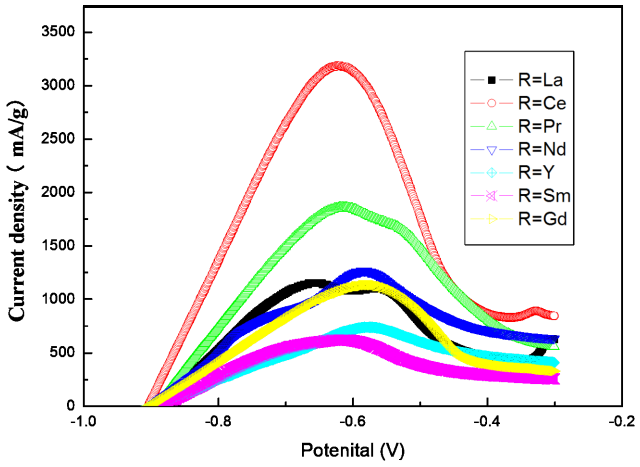

Figure 11. The anodic polarization curves of $La_{0.63}R_{0.2}Mg_{0.17}Ni_{3.1}Co_{0.3}Al_{0.1}$ alloy electrodes at 50% DOD and 293K.

Moreover, the Ce-, Pr-, Nd- and Gd-substituted have much larger limiting current density (I_L), indicating their larger hydrogen diffusion at electrode surface.

4. CONCLUSION

In this work, the structure and electrochemical properties of different R-substituted alloys have been studied systematically. Some conclusion can be summarized :

1) The XRD patterns and EPMA–WDS analysis show that the alloys consist mainly of La_2Ni_7 (Ce_2Ni_7-type, SG: $P6_3/mmc$) phase and minor $LaNi_5$ ($CaCu_5$-type, SG:P6/mmm) phase.
2) The thermodynamic and electrochemical properties are correlated to the crystallographic parameters. It is found that the equilibrium desorption hydrogen pressure and the maximum discharge capacity have some correlation to the unit cell volume.
3) The equilibrium pressure and electrochemical capacity increases with Ce~Gd substitution for La. However, Pr ~ Gd substitution improves the cycling stability. The capacity retention rate at the 100th cycle of Gd-substituted alloy rises by 23.6%.
4) Ce, Pr and Gd substitution greatly improves hydrogen diffusion rate in the bulk and charge transfer rate at the surface, and thus ameliorates the high rate discharge-ability. The HRD at 900mAg^{-1} reaches 78.4%, 220% higher than those of the original alloy for the Ce-substituted alloy.

5. ACKNOWLEDGEMENTS

This work was supported by the National Nature Science Foundation of China (No. 50941019) and Doctor Foundation of Binzhou University (2009Y02).

REFERENCES

[1] Winter Carl-Jochen, Int. J. Hydrogen Energy, 29, 1095 (2004).
[2] Sakai T, Matsuoka, M, Iwakura, C. Handbook on the Physics and Chemistry of Rare Earths. In: Eyring L, editors. Rare earth intermetallics for metal-hydrogen batteries, Amsterdam: Elesvier; 1995, p.133-78.
[3] Feng F., Geng M., Northwood D.O., Int. J. Hydrogen Energy, 26, 725 (2001).
[4] Liu F.J., Suda S., J. Alloys Comp., 232, 232 (1996).
[5] Reilly JJ., Handbook of Battery Materials. In: Besenhard JO, editors. Metal Hydrides Electrode, New York: Wiley; 2000, p.239-68.
[6] Zhao XY., Ma LQ., Shen XD., J. Mater. Chem., 22, 277 (2012).
[7] Kadir K., Sakai T., Uehara I., J. Alloys Comp., 257, 115 (1997).
[8] Kadir K., Sakai T., Uehara I., J. Alloys Comp., 302, 112 (2000).
[9] Kohno T., Yoshida H., Kawashima F., Inaba T., Sakai I., Yamamoto M, et al., J. Alloys Comp., 311, L5 (2000).
[10]Zhang FL., Luo YC., Chen JP., Yan RX., Chen JH., J. Alloys Compd., 430, 302 (2007).
[11]Iwase K., Sakaki K., Nakamura Y., Akiba E., Inorg. Chem., 49, 8763 (2010).
[12]Chai YJ., Asano K., Sakaki K., Enoki H., Akiba E., J. Alloys Compd., 485, 174 (2009).
[13]Chai YJ., Sakaki K., Asano K., Enoki H., Akiba E., Kohno T., Scr. Mater., 57, 545 (2007).
[14]Ferey A., Cuevas F., Latroche M., Knosp B., Bernard P., Electrochim. Acta, 54, 1710 (2009).
[15]Hayakawa H., Akiba E., Gotoh M., Kohno T., Mater. Trans., 46, 1393 (2005).
[16]Nakamura J., Iwase K., Hayakawa H., Nakamura Y., Akiba E., J. Phys. Chem. C, 113, 5853 (2009).
[17]Nakamura Y., Nakamura J., Iwase K., Akiba E., Nucl. Instrum. Meth. A, 600, 297 (2009).
[18]Ozaki T., Kanemoto M., Kakeya T., Kitano Y., Kuzuhara M., Watada M. et al., J. Alloys Compd., 446, 620 (2007).
[19]Zhang QA., Fang MH., Si TZ., Fang F., Sun DL., Ouyang LZ.

et al., J. Phys. Chem. C, 114, 11686 (2010).
[20]Zhang FL., Luo YC., Chen JP., Yan RX., Kang L., Chen JH., J. Power Sources, 150, 247 (2005).
[21]Zhang FL., Luo YC, Sun K, Wang DH, Yan RX, Kang L, et al., J. Alloys Compd., 424, 218 (2006).
[22]Zhang FL., Luo YC., Wang DH., Yan RX., Kang L., Chen JH., J Alloys Compd., 439, 181 (2007).
[23]Zhang J., Fang F., Zheng SY., Zhu J., Chen GR., Sun DL., et al., J. Power Sources, 172, 446 (2007).
[24]Denys RV., Yartys VA., Sato M., Riabov AB., Delaplane RG., J. Solid State Chem., 180, 2566 (2007).
[25]Filinchuk YE., Yvon K., Emerich H., Tetrahedral D., Inorg. Chem., 46, 2914 (2007).
[26]Denys RV., Riabov AB., Černý R., Koval'chuk IV, Zavaliy IYu., J. Solid State Chem., 187, 1 (2012).
[27]Yartys VA., Riabov AB., Denys RV., Sato M., Delaplane RG., J. Alloys Comp., 408, 273 (2006).
[28]Denys RV., Riabov AB., Yartys VA., Sato M., Delaplane RG., J. Solid State Chem., 181, 812 (2008).
[29]Guzik MN., Hauback BC., Yvon K., J. Solid State Chem., 186, 9 (2012).
[30]Buschow KHJ., Van Der Goot AS., J. Less-Comm Mat., 22, 419 (1970).
[31]van Vucht JHN., Kuijpers FA., Bruning HCAM., Philips Res. Rep., 25, 133 (1970).
[32]Young RA., Rietveld Method. In: Roung RA, editors. Introduction to the Rietveld Method, New York: Oxford University Press Inc, 1995, p. 1-38.
[33]Rodriguez-Carvajal J. In: Abstract of the Satellite Meeting on Powder Diffraction. Congress of the International Union of Crystallography. Toulouse, France, 1990, p.127; Fullprof Program, Version 3.5d October 98-LLB-JRC, 1998.
[34]Yuan HP., Zou ZY., Li ZN., Jiang LJ., Wang SM., Liu XP., et al., Int. J. Hydrogen Energy, 38, 7881 (2013).
[35]Naito K., Nastsunami N., Shukla AK., J. Power Sources, 63, 203 (1996).
[36]Notten PHL., Hokkeling P., J. Electrochem. Soc., 138, 1877 (1991).